A nonsequential turbulent mixing process

J. Duplat,[1] C. Innocenti,[2] and E. Villermaux[3,a)]
[1]*IUSTI, Aix-Marseille Université, 13453 Marseille Cedex 13, France*
[2]*Department of Physics, University of Florence, Florence 50019, Italy*
[3]*IRPHE, Aix-Marseille Université, 13384 Marseille Cedex 13, France*

(Received 10 February 2009; accepted 7 December 2009; published online 15 March 2010)

We study the relaxation of an initially segregated scalar mixture in a randomly stirred medium, aiming at describing the overall concentration distribution of the mixture, its shape, and its rate of deformation as it evolves toward uniformity. An ever dispersing mixture is realized by releasing a plume of scalar in a large scale, sustained turbulent medium on the axis and in the far field of a turbulent jet. The fluid particles constitutive of the plume are soon resolved into a set of stretched sheets whose rates of diffusive smoothing build up the overall mixture concentration distribution. The randomness of the particle's net elongation at a given instant of time induces a distribution of the mixing time from which molecular diffusion becomes effective in erasing the concentration differences. This ingredient is shown to rule the composition of this dispersing mixture, providing a detailed analytic description of the overall concentration distribution. It compares favorably with experiments using three different passive scalars, suggesting that the mixture composition results from a nonsequential, one-step lengthening process distributed among the sheets. © *2010 American Institute of Physics*. [doi:10.1063/1.3319821]

I. INTRODUCTION

A mixture is a transient state between the initial segregation of the constituents and their ultimate homogeneity. The constituents are segregated as long as they stand at distinct spatial locations at the molecular level; homogeneity is an appreciation of the residual concentration fluctuations of the constituents in the mixture compared to their mean.

We discuss how the normalized histogram $P(C,t)$ of the concentration content of a mixture deforms throughout the stirring process, aiming at describing the fraction of the fluid particles in the mixture $P(C,t)dC$ which bear a concentration level between C and $C+dC$ at time t. To this respect, the literature is rich of a number of interestingly convergent observations, albeit made in quite different systems. The concentration distribution $P(C,t)$ presents, in general, a bell shape centered around its average, except for extreme cases including the one discussed here; it is usually skewed and presents broad, exponential-like tails. These observations are common place in various instances including turbulent convection,[1] grid turbulence,[2–4] shear layers, jets,[5] randomly stirred two-dimensional flows[6–8] and three-dimensional flows,[9] polymer solutions,[10] and microfluidic devices[11,12] to quote a few among many examples.

Recent developments on scalar turbulence have emphasized the distribution of histories among the particles in stirred mixtures, specifically the distribution of stretching histories between initially nearby particles. In particular,[13–19] these broad concentration distributions are interpreted as reflecting the fluctuations in the stretching induced elongation of the fluid particles along their path in the fluid,[20] thus giving rise to a distribution of the time when molecular diffusion becomes effective,[21] and therefore to a distribution of concentration. The same lines of thought relating the Lagrangian trajectories of particles in the flow and global statistics have succeeded in describing the statistics of concentration *differences* in the medium.[22,23]

Yet, if some studies have concluded that a sequential cascade of essentially uncorrelated stretching is an appropriate paradigm for scalar mixing in more or less random flows, may they be turbulent, or chaotic,[14,15,17,24–26] some others have drawn the attention on permanent structures of unmixed regions slowing down the rate of concentration decay[18,19,27,28] or, on the contrary, on the existence of efficient "bypasses" making the cascade transparent.[29,30]

Here, we show that for a plume released in a sustained turbulent medium, the shape and the rate of deformation of $P(C,t)$, where increasing time t refers to increasing distances from the source, the mean-field sequential cascade picture is not appropriate, but that instead the mixture composition results from a nonsequential, one-step lengthening process distributed among the particles. This conclusion is reached by confronting experimental findings and the constraints they induce, with different mixing scenarios.

II. AN EVER DISPERSING MIXTURE

A plume of scalar is released in a large scale, sustained turbulent medium on the axis and in the far field of a turbulent jet in which it is free to disperse while it mixes.[29,31] As it is seen in Fig. 1, which displays an instantaneous planar cut through the field, the support of the scalar rapidly takes the form of an intermittent set of stretched sheets separated by larger and larger voids, some of the sheets possibly coalescing as they spread out and fade away. Figure 1 also illustrates that at a given location in the flow and even far from the

a)Electronic mail: villermaux@irphe.univ-mrs.fr. Also at Institut Universitaire de France.

FIG. 1. A snapshot of a dispersing plume made by the injection of a dye through a small tube of $d=8$ mm in diameter on the axis of a larger turbulent jet whose integral scale is $L=8$ cm at the injection location: $\mathrm{Re}=u'L/\nu=10^4$.

injection exit coexist sheets which bear a concentration close to the injection concentration and sheets which are almost fading away in the diluting medium.

A. Flow configuration and measurement methods

The plume is injected continuously in the far field and on the axis of a turbulent jet via a small tube whose diameter d is smaller than the local integral scale L. We have mainly used three tubes such that $d/L=0.05$, 0.1, and 0.16. The injection tube is placed 30–50 diameters downstream of the turbulence generator jet exit. The local integral scale is of the order of $L=6$ cm–8 cm and the root mean square (rms) velocity u' is about 25% of the mean velocity u, giving a turbulent Reynolds number $\mathrm{Re}=u'L/\nu=6000$ for $u=0.4$ m/s and $\mathrm{Re}=u'L/\nu=12\,000$ for $u=0.8$ m/s, where ν denotes the fluid kinematic viscosity. The injection point behaves neither as a source, nor as a sink of momentum, in the mean since the injection velocity u_{inj} through the injection tube is set equal to the average flow velocity u. The properties of the flow (stirring scale L and rms velocity u') are constant during the uniformization period of the scalar. The presence of the injection tube was checked to perturb a region of not more than 2 diameters.[29]

These experiments have been repeated with three types of scalars aiming at varying the intrinsic diffusive properties of the scalar being mixed and quantify its impact on the process, by varying the Schmidt number $\mathrm{Sc}=\nu/D$, where D is the scalar diffusivity. The scalars were temperature in air (Sc=0.7), temperature in water (Sc=7), and the concentration of disodium fluorescein in water (Sc=2000).

Point measurements of the concentration and temperature are made by a fiber optics probe, a cold film thermometer, and a cold wire thermometer, respectively. The optical probe is made of two 100 μm optical fibers positioned at right angle. One fiber illuminates the medium seeded with dye, and the other collects the fluorescence signal whose intensity is measured by a photodiode. The overall signal to noise ratio is over 50. Temperature in water was measured by a 250 μm cold film, providing an overall signal to noise ratio of about 100. Temperature in air was measured by a 1 μm in diameter and 200 μm in length cold wire with a signal to noise ratio larger than 100. The signals were further amplified and digitized by a 16 bits A/D converter. The resolution of the probes matches the Kolmogorov scale, in all cases.

Planar measurements of the fluorescent scalar field were done by shining a plane, monomode (488 nm) argon laser sheet through the water tank in a plane containing the axis of the mean flow. The images were recorded by a cooled, 12 bits, 1280×1024 pixels wide digital camera. All these experiments are made using low concentration levels of dye ($C_0=10^{-4}$ mol l^{-1}) with no appreciable attenuation on the corresponding optical path and weak temperature differences so that the scalars are always passively advected by the flow. The relative density differences $\Delta\rho/\rho$ due to the presence of dye, or heated fluid particles, are such that the associated buoyancy effects are sensitive on a length scale $\ell_B=u\sqrt{\rho L/\Delta\rho g}$ of the order of 10 m, much larger that the setup typical size. In the following, distances are counted in the direction downstream from the scalar injection location, and we relate space to time by

$$x=ut, \tag{1}$$

where u is the mean flow convection velocity. Concentrations are normalized by the injection concentration so that C stands for C/C_0.

B. Concentration content

The distribution of concentration $P(C)$ is measured on the centerline of the main turbulent jet at various downstream distances. Since the scalar plume meanders in the radial direction, these measurements made at locations fixed in space probe the entire concentration levels available in the distribution $P(C)$ at each position. The traces of the concentration signal recorded in three distinct experiments with Sc=2000, 7, and 0.7 at $x/d=10$ display the expected trend that the concentration fluctuations are weaker when the dye is more diffusive (Figs. 2–4).

As seen in Fig. 3, the distributions $P(C)$ exhibit a cusped shape at the origin close to the concentration at the diluting concentration $C=0$. That cusp is followed by an exponential-like behavior around an inflexion point (Fig. 5) which itself

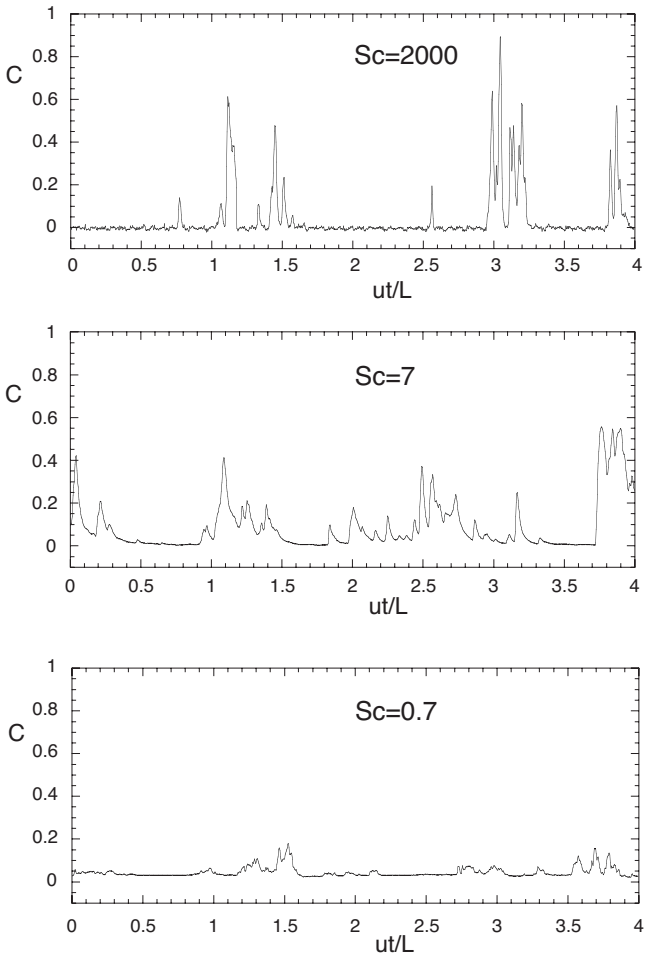

FIG. 2. Temporal traces of the concentration signal recorded at $x/d=10$ and converted, with Taylor hypothesis, to instantaneous one-dimensional cuts of the concentration field, for three different Schmidt numbers Sc=2000, 7, and 0.7 with $d/L=0.05$.

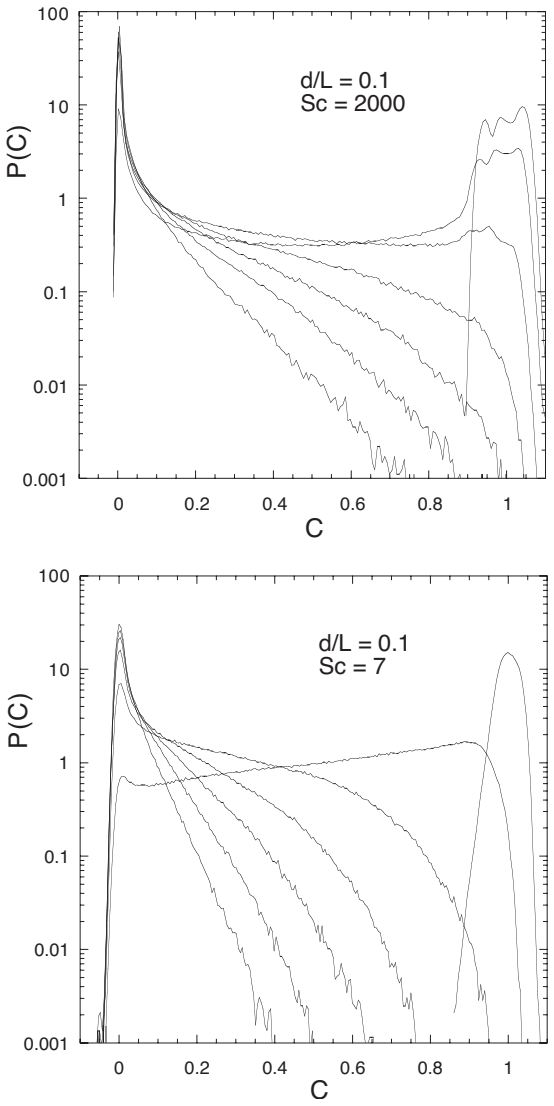

FIG. 3. Evolution of the concentration distribution $P(C)$ of the ever dispersing mixture shown in Fig. 1 for increasing distances from the injection point $x/d=0,2.5,5,7.5,10,12.5,15$, and two distinct Schmidt numbers at $\mathrm{Re}=10^4$. Negative temperatures are reminiscent of the ambient temperature noise. The steeper the distribution, the larger x/d is.

precedes a rapid fall-off for larger values of C at the tail of the distribution (see also Ref. 32, downstream of a line source in grid turbulence). The argument of the exponential tangent at the inflexion point steepens with downstream distance as

$$P(C) \sim \exp(-\alpha C) \quad \text{with} \quad \alpha = \frac{x/d}{f(\mathrm{Sc})}, \tag{2}$$

where $f(\mathrm{Sc})$ is a slowly increasing function of the Schmidt number. Indeed, as also shown in Fig. 5, the slopes of these exponentials tangent to $P(C)$ at the inflexion point depend, for a given value of x/d, on the dye diffusivity; a fit consistent with the data is a weak power law $f(\mathrm{Sc}) \sim \mathrm{Sc}^{1/5}$, although a logarithmic dependence, $f(\mathrm{Sc}) \sim \ln(\mathrm{Sc})$, is not inconsistent as well (see Sec. IV and Fig. 6). The use of three different injection diameters indicates that d is actually the relevant length scale, which sets the argument of the exponential decrease and of the overall shape of the distribution. In particular, Fig. 7 shows that this length scale is *not* equal to $d^{2/3}L^{1/3}$, i.e.,

$$\alpha \neq x/(d^{2/3}L^{1/3}) \tag{3}$$

as one would have expected from a naive Kolmogorov scaling assuming that the time it takes to cascade from d to dissipative scales is $d/(\epsilon d)^{1/3}$ with $\epsilon = u'^3/L$. Nor is this length scale equal to L itself, i.e.,

$$\alpha \neq x/L \tag{4}$$

as one would have expected if the large scale shear sustained by the main jet would have been dominant. A further discussion on the kinetics of the process is given in Sec. IV.

This scaling dependency is apparent as well on the first moment of $P(C)$, namely, the average concentration

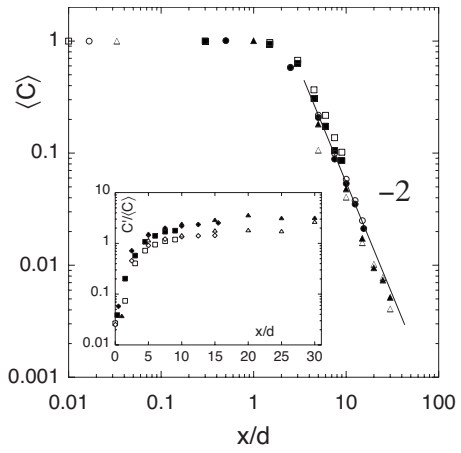

FIG. 4. Downstream evolution of the average concentration $\langle C\rangle$ in the ever dispersing mixture of Fig. 1 for three different injection diameters and two Schmidt numbers. Inset: downstream evolution of the fluctuations $C'/\langle C\rangle = \sqrt{\langle C^2\rangle/\langle C\rangle^2 - 1}$, Re=6000. d/L=0.05 (▲), 0.1 (■), 0.16 (●), Sc=2000. For Sc=7, the same opened symbols.

$$\langle C\rangle = \int CP(C)dC, \tag{5}$$

whose downstream evolution is shown in Fig. 4 in the scaled coordinates x/d for three different injection diameters. The asymptotic trend is consistent with

$$\langle C\rangle \sim \left(\frac{x}{d}\right)^{-2}, \tag{6}$$

independent of the Schmidt number. This relation is an immediate consequence of the continuity of the scalar flux, advected at a mean velocity u and issuing in the medium from a section of diameter d. The radius of exploration of the plume downstream of the tube exit increases in proportion to the distance x for $x<L$ as a result of the persistent ballistic

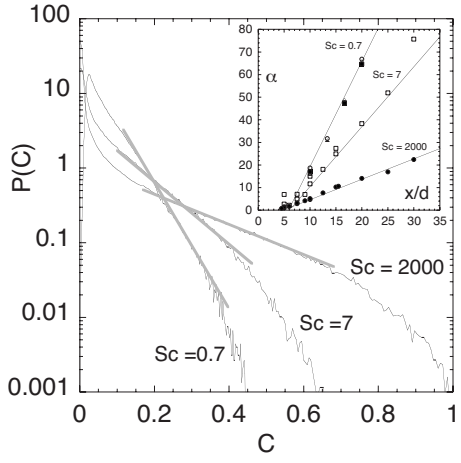

FIG. 5. Concentration distributions $P(C)$ of the ever dispersing mixture of Fig. 1 recorded at x/d=10 for three different Schmidt numbers. The shape of the distributions is exponential near the gray shades regions like $P(C)\sim\exp(-\alpha C)$. Inset: the argument α for different downstream locations x/d, Reynolds numbers, and three Schmidt numbers. ●: Sc=2000, Re=6000 and 12 000, d/L=0.05,0.1,0.6. □: Sc=7, Re=6000, d/L=0.05,0.1,0.16. ■: Sc=0.7, d/L=0.08, Re=23 000; ○, △: Sc=0.7, d/L=0.08, Re=45 000.

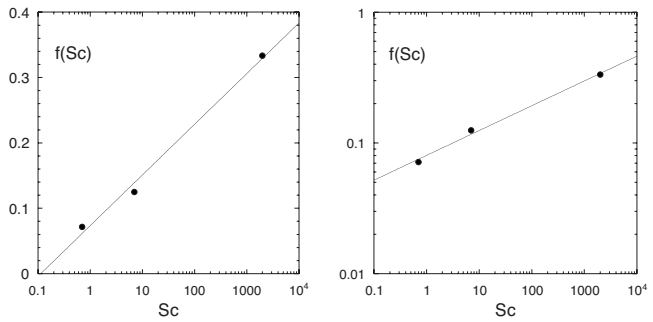

FIG. 6. Dependence on the Schmidt number f(Sc) of the argument α in the exponential wings at the inflexion point of the distributions $P(C)$ in Eq. (2). Left: logarithmic adjustment. Right: power law adjustment. The line has a slope equal to 1/5. See also the discussion in Sec. II D.

motion within one integral turnover time,[33] hence providing the equation above (see also Ref. 31). In particular, the exponent −2 has a purely geometrical origin. It would be −1 immediately downstream of a line source for $x<L$ and −1/2 for $x\gg L$ in the normal diffusive regime (see, e.g., the measurements in Ref. 32). Because of this geometrical constraint, it is thus not surprising that the downstream evolution of the mean concentration in Eq. (6) is independent of the Schmidt number.

C. Material contours

Stirring motions increase the length of material lines. We quantify the increase in the scalar support contour length from the two-dimensional slices through the field by a procedure illustrated in Fig. 8, which holds for both the dispersing, and confined mixtures.

From a large number of images of the field like the one in Fig. 8, we compute the amount of contour length $\ell(x)$ within a window of width ℓ_0 around each downstream location x when the field has been thresholded at a given concentration C_s. The threshold concentration C_s may be kept constant for all downstream locations, or may be adjusted such that the contour contains a given fraction of the whole field. Specifically, the contour may be defined at each x location such that

$$C_s(x) = C^{\mathrm{st}} \quad \text{or} \quad \int_0^{C_s(x)} P(C,x)dC = C^{\mathrm{st}}, \tag{7}$$

the constants being equal to a fraction determined *a priori*. The evolution of contour lengths according to the first rule $[C_s(x)=C^{\mathrm{st}}]$ were studied by Villermaux *et al.*[31] in the ever dispersing mixture. In that case, the length first increases as a consequence of the motions in the flow and then, as the concentration levels diminish, decreases. The fraction of the fluid particle in the mixture whose concentration has remained above the threshold at a given location x diminishes as well with x. The trend is independent of the choice of C_s, only the chronology is (Fig. 9).

Here, we have also examined the case when the threshold concentration is adjusted for the contour to concern a fixed fraction of the fluid particles in the mixture. We find that the early increase in the amount of contour within ℓ_0 is

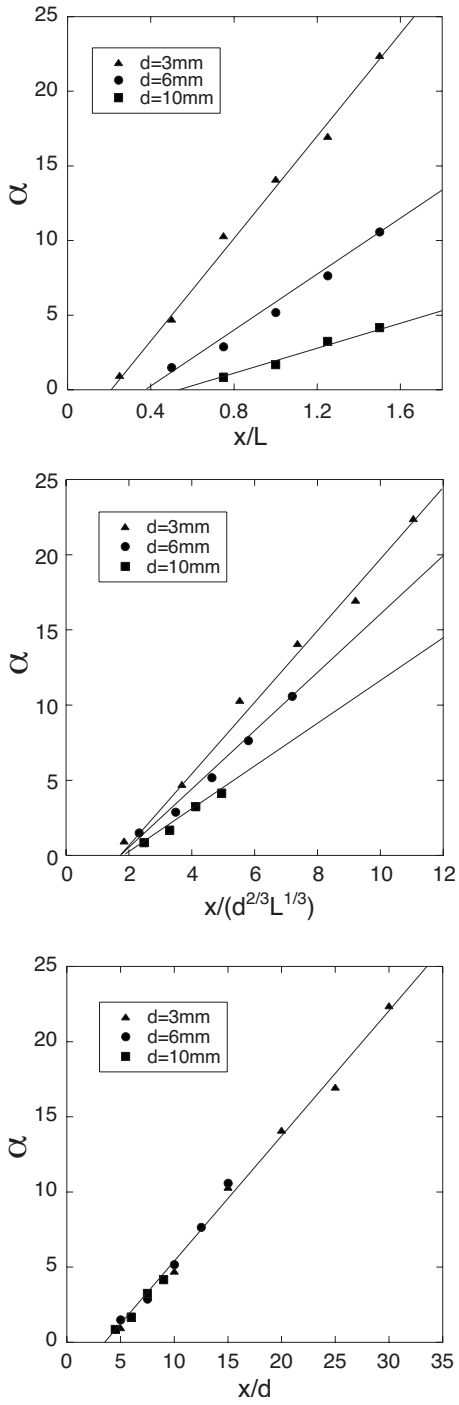

FIG. 7. Comparison of different possible scalings for α in Eq. (2): Sc=2000.

superimposed on that of the fixed threshold rule, and that the increase goes on in a linear fashion with downstream distance.

Before the concentration levels of the sheets have decreased [i.e., for $t<t_s$, where t_s is the mixing time defined by Eq. (24)], the contour surface is a material surface, and its deformation reflects the dispersion properties of the underlying flow. Thus, a direct way to understand the linear increase in the contour length is to consider the separation velocity (or pair dispersion) $\Delta r/\Delta t$ between two material points separated by r, that we take for simplicity here as

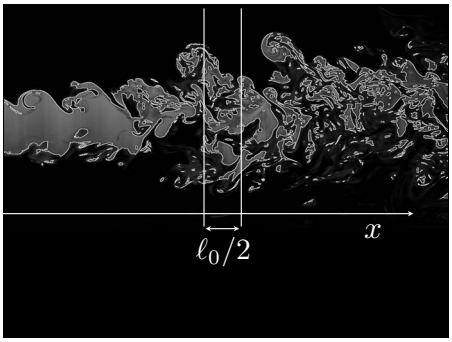

FIG. 8. An example of contour length extraction when the threshold concentration $C_s(x)$ is adjusted for the contour to concern a fixed fraction of the fluid particles in the mixture at each location x, namely, $\int_0^{C_s(x)} P(C,x)dC=0.93$.

$$\left\langle \frac{\Delta r}{\Delta t} \right\rangle = \gamma(t) r \tag{8}$$

on ensemble average, where $\gamma(t)$ is a-possibly time-dependent-stretching rate.

Let $N(r,t)$ be the number of segments of length r needed to cover the contour of a material element at time t. The element current length viewed at scale r is thus $\ell(r,t)=rN(r,t)$. Conservation of the number of segments stretched by the base flow writes $N(r+\Delta r,t+\Delta t)=N(r,t)$ and gives

$$\frac{\partial N}{\partial t} + \left\langle \frac{\Delta r}{\Delta t} \right\rangle \frac{\partial N}{\partial r} = 0. \tag{9}$$

With $\tau(t)=\int_0^t \gamma(t')dt'$, Eqs. (9) and (8) amount to

$$\frac{\partial N}{\partial \tau} + \frac{\partial N}{\partial \ln(r)} = 0, \tag{10}$$

indicating that $N(r,t)$ propagates at speed unity in the $\{\ln(r),\tau\}$ space. Solutions are thus of the form $N(r,t)=f[\ln(r)-\tau]$. For an initially smooth contour

$$N(r,t=0) = \frac{\ell_0}{r}, \tag{11}$$

one has at any posterior time t

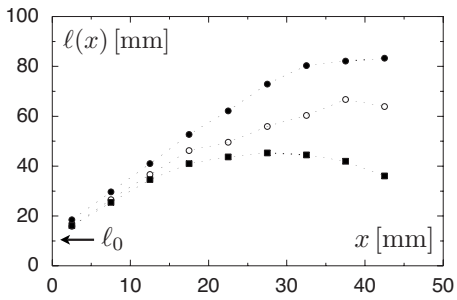

FIG. 9. Downstream increase of contour lengths $\ell(x)$ measured in a window of width $\ell_0/2=5$ mm and averaged over many realizations, represented versus downstream distance x, for three different injection diameters: ●: $d=10$ mm; ○: $d=6$ mm; ■: $d=3$ mm. The contours are extracted with a constant concentration threshold $C_s\approx 0.9$.

$$N(r,t) = \frac{\ell_0}{r}\exp\left[\int_0^t \gamma(t')dt'\right]. \quad (12)$$

A more refined scale dependence in Eq. (8) would in addition account for the *fractal* character of the contour,[34] with a dimension $-d \ln N(r,t)/dr$ depending on scale r (Ref. 35) and increasing as time elapses.[31]

The increase in the net material blob contour length therefore defines the effective stretching rate $\gamma(t)$. A constant stretching rate $\gamma(t) \equiv \gamma$ will obviously lead to exponential growth. Let $\gamma(t) = \beta\sigma/(1+\sigma t)$, where σ is some elongation rate, one expects in that case

$$\ell(t) = \lim_{r\to 0}\{rN(r,t)\} = \ell_0(1+\sigma t)^{\beta}. \quad (13)$$

The observations reported in Fig. 9 indicate that

$$\ell(x) - \ell_0 \sim x, \quad (14)$$

independent of the injection diameter d. Therefore, one has from Eq. (13), $\beta=1$ and, with $x=ut$, the effective stretching rate

$$\gamma(t) = \frac{\sigma}{1+\sigma t} \quad (15)$$

and elongation rate

$$\sigma = \frac{u}{d}. \quad (16)$$

Independent measurements of the pair dispersion made in the same flow confirm the linear temporal increase of the distance between pairs of particles.

As the mixture disperses and mixes, the length of a contour bordering a fixed fraction of the mixture increases in proportion to time. Conversely, since these measurements have been done on two-dimensional slices through a three-dimensional field, it is believable, that surfaces of material elements increase like $\ell(t)^2 \sim t^2$ (see also Ref. 5 in a related shear flow presenting that same property).

D. Stretching enhanced diffusion

Focus at the scale of the elementary scalar sheets visible from the intercept with the visualization plane (Fig. 1). It is known that a succession of random stretching motions applied to passive objects form sheets[36–38] for which there is a number of experimental evidences (see Refs. 39 and 40 among others). Let us consider a *single* sheet, and let C be the scalar concentration in the vicinity of the sheet and z a coordinate in the direction normal to the isoconcentration surface C. The diffusive uniformization of the dye is enhanced by the stretching of the underlying motions. The convection-diffusion transport equation for C reduces (see, e.g., Refs. 39 and 41–50) to a one-dimensional problem when the radius of curvature of the isoconcentration surface is large compared to the lamella thickness.[51] Let $s(t)$ be the distance between two material particles in the direction z perpendicular to a sheet, and

$$\gamma_c(t) = \frac{\mathrm{d}\,\ln\{s(t)\}}{\mathrm{d}t} \quad (17)$$

its rate of compression. The mass conservation equation of a species with diffusion coefficient D then writes as

$$\frac{\partial C}{\partial t} + \gamma_c(t) z \frac{\partial C}{\partial z} = D\frac{\partial^2 C}{\partial z^2}. \quad (18)$$

By the change in variables

$$\tau = D\int_0^t \frac{\mathrm{d}t'}{s(t')^2} \quad \text{and} \quad \xi = \frac{z}{s(t)}. \quad (19)$$

Equation (18) is reduced to a simple diffusion equation,

$$\frac{\partial C}{\partial \tau} = \frac{\partial^2 C}{\partial \xi^2}. \quad (20)$$

Suppose that the lamellas have an initial width s_0 and uniform concentration so that its concentration profile is a "top hat." At any later time, its concentration profile is the solution of equation[19] (see, e.g., Refs. 5 and 49) from which it follows that the maximal concentration in the lamellae is

$$C(0,t) = \mathrm{erf}\left(\frac{1}{4\sqrt{\tau}}\right). \quad (21)$$

With

$$s(t) = \frac{s_0}{(1+\sigma t)^2} \quad (22)$$

as implied, using mass conservation $\ell(t)^2 s(t) \sim s_0^3$ (or, equivalently, $\gamma_c = -2\gamma$), by the experimentally observed linear increase in material contours lengths and from Eq. (19),

$$\tau = \frac{1}{5\ \mathrm{Pe}}(-1+(1+\sigma t)^5) \quad \text{with} \quad \mathrm{Pe} = \frac{\sigma s_0^2}{D}. \quad (23)$$

The mixing time t_s, reached when $\tau = \mathcal{O}(1)$ is thus, when the Péclet number (Pe) is larger than unity

$$t_s \sim \frac{1}{\sigma}\mathrm{Pe}^{1/5} \quad \text{and} \quad C(0,t) \sim \left(\frac{t}{t_s}\right)^{-5/2} \quad \text{for } t > t_s. \quad (24)$$

If the flow were stretching lines exponentially fast so that $s_0 e^{-\sigma t}$, one would have

$$t_s = \frac{1}{2\sigma}\ln \mathrm{Pe} \quad \text{and} \quad C(0,t) = e^{-\sigma(t-t_s)}. \quad (25)$$

III. DISTRIBUTED INDIVIDUAL TRAJECTORIES

Our reasoning has up to now involved a single elongation rate σ and therefore a single mixing time t_s. The measurement of the elongation of material contours provides an average of the elongation rate. We now consider possible fluctuations in the net elongation between the fluid particles in the medium, fluctuations whose natural consequence is the *distribution of the mixing times* themselves. This phenomenon is obvious from Fig. 1: at a given location in the flow coexist sheets which still bear the injection concentration and sheets which are almost fading away in the diluting medium.

A. Distribution of elongations

We now envisage this ingredient and examine its consequences on the shape of $P(C)$. Regarding turbulent, random flows, the fundamental question to ask is whether the distribution of elongation among fluid particles at a *fixed time* results from a *sequential process* with many independent steps, or from a *single event* distributed in intensity. Another less important aspect is whether the flow is of a *stretching* type, that is if material lengths increase exponentially in time, or of a *lengthening* type, that is if material lengths grow algebraically. Starting with a collection of identical particles of size ℓ_0, they will fall in a distribution of elongation $\mathcal{P}(\ell,t)$ an instant of time t later whose two first moments, either on a linear scale

$$\langle \ell \rangle = \int \ell \mathcal{P}(\ell,t) d\ell \quad \text{and} \quad \sigma_\ell^2 = \langle \ell^2 \rangle - \langle \ell \rangle^2 \tag{26}$$

or on a logarithmic scale

$$\langle \ln \ell \rangle = \int \ln(\ell) \mathcal{P}(\ell,t) d\ell \quad \text{and} \quad \sigma_{\ln \ell}^2 = \langle \ln(\ell)^2 \rangle - \langle \ln(\ell) \rangle^2 \tag{27}$$

define its width relative to its mean. Several scenarios may arise. We describe some of them, explore the consequences on the evolution of material lengths, and compare with our experimental findings.

(1) *One step lengthening.* Let $\ell = \ell_0(1+\sigma t)$, with the elongation rate σ distributed (different particles are lengthened at different rates, but for each fluid particle the elongation rate is constant). The distribution of length $\mathcal{P}(\ell,t) = 1/\ell_0 t P_\sigma((\ell/\ell_0 - 1)/t)$ is given by the distribution of σ. Consequently, $\mathcal{P}(\ell,t)$ is self-similar in ℓ as time t is varied, and the moments grow in time as $\langle \ell \rangle \sim t$, $\sigma_\ell \sim t$, $\langle \ln \ell \rangle \sim \ln t$, and $\sigma_{\ln \ell} \sim C^{te}$ [$\ln(\ell)$ is a random variable distributed like $\ln(\sigma)$ and σ has a stationary distribution]. Measurements and numerical simulations in various chaotic flows by Muzzio and Ottino (see, e.g., Ref. 52 and references therein) indicate that the distribution of the elongation ℓ/ℓ_0 does tend asymptotically, in this context, toward a bell-shape curve translated self-similarly in log-log coordinates.

(2) *One step stretching.* Let $\ell = \ell_0 \exp(\gamma t)$, with the stretching rate γ fixed but distributed among the different particles. The distribution of length $\mathcal{P}(\ell,t) = 1/(\ell t) P_\gamma[\ln(\ell/\ell_0)/t]$ gets broader with time. The distribution of $\ln(\ell)$ is similar to P_γ, and one has $\langle \ln(\ell) \rangle \sim t$ and $\sigma_{\ln(\ell)} \sim t$. The mean length $\langle \ell \rangle$ grows faster than exponentially since it is more and more impacted by higher stretching rates: for instance, with P_γ Gaussian with mean $\langle \gamma \rangle$ and variance σ_γ^2, one has $\langle \ell \rangle \sim \int d\gamma \exp(\gamma t) \exp[-(\gamma - \langle \gamma \rangle)^2/2\sigma_\gamma^2]$, i.e., $\langle \ell \rangle \sim \exp(\langle \gamma \rangle t + \sigma_\gamma^2 t^2/2)$ and $\sigma_\ell \sim \exp(\langle \gamma \rangle t + \sigma_\gamma^2 t^2)$.

(3) *Multistep lengthening with steps defined on determined time intervals and stationary elongation distribution.* Let $d\ell/dt = \sigma_i$ with the elongation σ_i fixed for one particle during the time interval $[t_i t_{i+1}]$. This is a typical case for application of the central limit theorem: if the distribution of elongation is independent of time, and the time intervals have a constant duration, the distribution $\mathcal{P}(\ell,t)$ at large t is nearly Gaussian with $\langle \ell \rangle \sim t$ and $\langle \sigma_\ell \rangle \sim \sqrt{t}$.

(4) *Multistep stretching with steps defined on determined time intervals and stationary stretching distribution.* Let $d\ell/dt = \gamma_i \ell$ with the stretching γ_i fixed for one particle during the time interval $[t_i \ t_{i+1}]$. This is another typical case of application of the central limit theorem, applied for $\ln(\ell)$. If the distribution of stretching rates is independent of time, the distribution $\mathcal{P}(\ell,t)$ at large t is nearly log normal with $\langle \ln(\ell) \rangle \sim t$ and $\langle \sigma_{\ln(\ell)} \rangle \sim \sqrt{t}$. Taking $\mathcal{P}(\ell,t)$ as an exact lognormal distribution (i.e., if the stretching rates γ_i are Gaussians) leads to $\langle \ell \rangle \sim \exp(\langle \ln(\ell) \rangle + \sigma_{\ln(\ell)}^2/2) \sim \exp(at)$ and $\sigma_l \sim \exp(\langle \ln(\ell) \rangle + \sigma_{\ln(\ell)}) \sim \exp(bt)$ with $0 < a < b$ two positive constants.

(5) *Multistep stretching with steps defined on constant time intervals and decaying stretching rates.* Let $d\ell/dt = \gamma_i \ell$ with the stretching γ_i fixed for one particle during the time interval $[t_i \ t_{i+1}]$, and let the self-similar distribution of γ_i be given by $1/\langle \gamma_i \rangle P(\gamma_i/\langle \gamma_i \rangle)$. Let $\langle \gamma_i \rangle \sim t^{-a}$ be a decaying function of time. $\ln(\ell)$ is a sum of random variables with mean $\langle \ln(\ell) \rangle \sim \int t'^{-\alpha} dt'$ and variance $\sigma_{\ln(\ell)}^2 \sim \int dt' t'^{-2a}$. Then, for $1/2 < a \leq 1$ the variance of the sum tends to a finite limit as time tends to infinity, whereas its mean diverges. The variance—and the shape—of the distribution of $\ln(\ell)$ is mostly determined by the first steps, and there is no convergence toward a Gaussian; besides, the mean $\langle \ln(\ell) \rangle$ may tend to infinity. In such decaying stretching process, the shape of the distribution $\mathcal{P}(\ell,t)$ is essentially fixed by the first steps. The subsequent events induce a narrowing of the distribution of stretching.

The distribution $\mathcal{P}(\ell,t)$ is nearly self-similar in ℓ as time t is varied and completely determined by the value of $\langle \ell(t) \rangle$. We can now exhibit two particular cases. If $\langle \gamma(t) \rangle = 1/t$, then $\langle \ell \rangle \sim t$ and one recovers case (1) above, whereas if $\langle \gamma(t) \rangle = 3/2t$, then $\langle \ell \rangle \sim t^{3/2}$, which is the classical Richardson dispersion.

This latter scenario is, however, very unlikely for turbulent flows: the particular behavior of $\mathcal{P}$ is not only due to the decay of the stretching rate but also to a specific choice for the temporal autocorrelation of the stretching: the correlation time of the stretching in this scenario is constant and is independent of the stretching rate.

(6) *Multistep stretching with decaying stretching rates, but a fixed persistency.* Stretching rates are broadly distributed in random flows.[53,54] However, what matters as far as material length growth is concerned is the product of the rate of stretch by its correlation time τ, which defines the persistency. The stretching of a material element in turbulent flows is likely to persist for a time inversely proportional to its intensity: most likely the stretching rate γ_i at the ith step is constant for a time τ_i such that $\gamma_i \tau_i \approx 1$.[38] In this scenario, the length attained after n steps is independent of the individual trajectory

$[\ell_n = \exp(n)\ell_0]$, but the time t_n spent to reach this length is distributed among the particles. It is then useful to introduce the probability $\mathcal{T}(\ell,t)$ as the distribution of time t needed to reach the length ℓ. This probability is unambiguously defined as soon as we consider that ℓ is a strictly increasing function of time so that for each trajectory there exist a unique correspondence between ℓ and t.

The relation between $\mathcal{T}$ and $\mathcal{P}$ can be obtained as follows. Let us consider a particular time t^* and a particular length ℓ^*. A certain proportion of fluid particles have a length larger than ℓ^*, at time t^* which, by definition of $\mathcal{P}$ is

$$\int_{\ell^*}^{\infty} \mathcal{P}(\ell,t^*)d\ell.$$

For these particles, the length ℓ^* was reached before the time t^* so that this proportion is also

$$\int_0^{t^*} \mathcal{T}(\ell^*,t)dt$$

and thus

$$\mathcal{P}(\ell^*,t^*) = -\frac{d}{d\ell}\left[\int_0^{t^*} \mathcal{T}(\ell,t)dt\right]\Bigg|_{\ell=\ell^*}. \tag{28}$$

The distribution of time $\mathcal{T}(\ell,t)$ is determined by the self-similar distribution of time τ_i associated with each steps $P_i(\tau_i) = 1/\langle\tau_i\rangle P(\tau_i/\langle\tau_i\rangle)$. The decrease in the stretching rate implies that $\langle\tau\rangle \sim l^a$ with $a>0$. As $\ell_i \sim \ell_0 \exp(i)$, we have $\tau_i \sim \tau_0 \exp(ai)$. After n steps, the average time is $\langle t\rangle \sim \tau_0[\exp(an)-1]/[\exp(a)-1]$. The last step lasts for a proportion $1-\exp(-a)$ of the total duration. The variance for time after n steps $\sigma_t^2 \sim \tau_0^2[\exp(2an)-1]/[\exp(2a)-1]$ is also mostly given by the last step for sufficient large a.

Then, for a stretching decaying sufficiently fast (i.e., for a sufficiently large) the distribution $\mathcal{T}(\ell,t)$ is nearly equal to the distribution for the last step. It is then characterized by a single time scale $\langle t_\ell\rangle$,

$$\mathcal{T}(\ell,t) = 1/\langle t_\ell\rangle P(t/\langle t_\ell\rangle).$$

Consequently,

$$\mathcal{P}(\ell,t) = \frac{d\langle t_\ell\rangle}{d\ell}\frac{1}{\langle t_\ell\rangle^2}P(t/\langle t_\ell\rangle). \tag{29}$$

The case $a=1$ corresponds to a linear growth of material lengths with time, whereas $a=2/3$ corresponds to a Richardson-type expansion ($\langle\ell^2\rangle \sim t^3$).

The scenarios described above do not cover all the possibilities but represent several relevant cases and limits. The experimental facts in Sec. II actually suggest that the overall statistical content of the ever dispersing mixture depends solely on a single, Schmidt dependent time scale since the distributions shapes are identical, albeit a rescaling involving Sc only (see Fig. 4), at a given location from the source. The width of the distribution is proportional to its mean. This self-similarity property rules out cases (3) and (4) listed above and since material lines grow linearly in time, only cases (1) and (6) remain as compatible candidates to represent $\mathcal{P}(\ell,t)$. We do not consider case (5) because of the varying persistency, which is unlikely in stationary flows.

These two cases [(1) and (6)] lead to similar behaviors for $\mathcal{P}(\ell,t)$ and $\mathcal{T}(\ell,t)$. The latter is fully determined by the mean time (t_ℓ) scaling like ℓ/u for a linear growth of material line with time. In that case, an obvious assumption is to postulate that the distribution of times to reach a length ℓ is such that

$$\int_T^{\infty} \mathcal{T}(\ell,t)dt = \lim_{\delta t\to 0}\left(1-\frac{\delta t}{\ell/u}\right)^{T/\delta t} = e^{-uT/\ell}, \tag{30}$$

according to the usual Poisson estimate so that

$$\mathcal{T}(\ell,t) = \frac{u}{\ell}e^{-ut/\ell} \tag{31}$$

and, equivalently, owing to Eq. (29) giving the distribution of elongations ℓ at time t as an *inverted gamma* distribution

$$\mathcal{P}(\ell,t) = \frac{ut}{\ell^2}e^{-ut/\ell} \tag{32}$$

sometimes encountered in other contexts.[55]

B. Distribution of mixing times

Associated with the distribution of the elongation ℓ is a distribution of the mixing times t_s. At a given instant of time, some particles have been more elongated than others because ℓ is distributed. As a result, some particles have not yet reached their mixing time because they have not been elongated enough and still bear the initial concentration, while some other, which are more elongated, have a concentration which has already started to decay. Indeed, $\mathcal{T}(\ell,t)$ is defined for all length ℓ and, in particular, for $\ell_s = u\langle t_s\rangle$ the elongation of the particle at the mixing time. Since $\mathcal{T}(\ell,t)$ is self-similar in time as ℓ is varied, $\mathcal{T}_s(t_s) = \mathcal{T}(\ell_s,t_s) = \langle t_s\rangle/\langle t_\ell\rangle\mathcal{T}(\ell,t_s\langle t_\ell\rangle/\langle t_s\rangle)$.

The construction and meaning of $\mathcal{T}_s(t_s)$ is very similar to the "distribution of doubling times,"[56,57] that is, the time it takes to increase the distance between two particles by a prescribed amount. It is also encountered in other contexts[58] and is found to have an exponential tail directly associated to the fact that the elongation events are Poisson distributed.

From Eq. (31), we thus have the distribution of mixing times as

$$\mathcal{T}_s(t_s) = \frac{1}{\langle t_s\rangle}\exp\left(-\frac{t_s}{\langle t_s\rangle}\right) \tag{33}$$

over the whole range of t_s, a distribution which was already obtained from similar arguments[13,59] or in the short time-correlation limit.[15] This expression for the distribution of mixing time is consistent with any one-step scenario [i.e., cases (1), (2), (5), and (6)].

We discuss below the distributions of elongation or stretching rate corresponding to the two remaining pertinent cases.

(a) In case (1), $\sigma=(\ell_s/\ell_0-1)/t_s$ so that σ is distributed as

$$P_\sigma(\sigma)=\frac{\ell_s/\ell_0-1}{\sigma^2\langle t_s\rangle}\exp\left(-\frac{\ell_s/\ell_0-1}{\sigma\langle t_s\rangle}\right).$$

(b) For case (6), $t_s\approx\tau_n\langle t_s\rangle/\langle\tau_n\rangle=\tau_n\ln(\ell_s/\ell_0)/\ln(\ell_n/\ell_{n-1})$ is approximately proportional to τ_n the duration of the last step. Since $\ell_n=\ell_{n-1}\exp(\gamma_n\tau_n)$,

$$P_\gamma(\gamma)=\frac{\ln(\ell_n/\ell_{n-1})}{\gamma^2\langle\tau_n\rangle}\exp\left[-\frac{\ln(\ell_n/\ell_{n-1})}{\gamma\langle\tau_n\rangle}\right],$$

which is the same distribution as in case (2). Another way of finding the same result is to note that since the persistency of a stretching event $\gamma\tau=1$ is fixed, the distribution of mixing times is dominated by the distribution of the last event, which lasts for a time τ. With τ distributed exponentially, the stretching rate is distributed like

$$P_\gamma(\gamma)=\frac{1}{\gamma^2\langle\tau\rangle}\exp\left(-\frac{1}{\gamma\langle\tau\rangle}\right),$$

a distribution presenting a bell shape around its maximum, a positive skewness, and a large power law tail for intense events. This shape is in qualitative agreement with the one found numerically[54] in a three-dimensional numerical simulation, or measured[53] in a two-dimensional weakly turbulent flow.

C. Concentration distribution

Finally, the distribution of concentration $P(C,t)$ is derived from similar arguments. Similar to the way $\mathcal{P}(\ell,t)$ is deduced from $\mathcal{T}(\ell,t)$, one may define $\mathcal{T}(C,t)$ as the distribution of time at which a certain level of concentration C is reached. Since C is a decreasing function of time,

$$P(C^*,t^*)=+\frac{d}{dC}\left[\int_0^{t^*}\mathcal{T}(C,t)dt\right]\Bigg|_{C=C^*}. \tag{34}$$

$\mathcal{T}(C,t)$ results from a one dominating step process, and is therefore a self-similar function of time, as the concentration C is varied. It is completely defined by the distribution of mixing time $\mathcal{T}_s(t_s)$ [see Eq. (33)] and the average time associated to each concentration level $\langle t_C\rangle$. The latter is given by the time dependence of the concentration $C(t)$ of a fluid particle before and after the mixing time given by the microscopic convection-diffusion problem. We have shown in Sec. II D that $C(t)$ remains close to 1 for $t\ll t_s$ and that $C(t)=(\sigma s_0^2/D)^{1/2}(\sigma t)^{-\nu}$ with $\nu=5/2$ for $t\gg t_s$. A convenient (but not restrictive) crossover function bridging these two extremes is

$$C(t)=\left(1+\frac{t}{t_s}\right)^{-\nu}, \tag{35}$$

leading to

$$\langle t_C\rangle=\langle t_s\rangle(C^{-1/\nu}-1), \tag{36}$$

and providing finally the concentration distribution $P(C,t)$ as a function of time

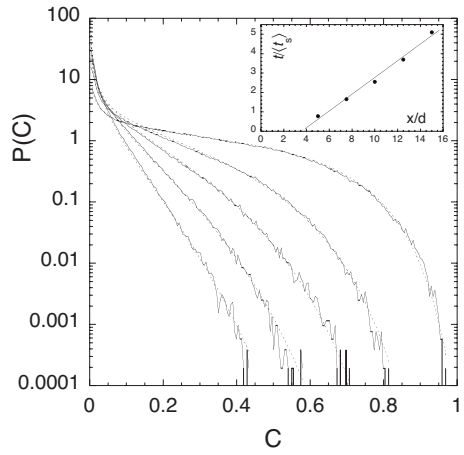

FIG. 10. Concentration distributions of the ever dispersing mixture recorded at $x/d=5$, 7.5,10,12.5, and 15 with $d=0.6$ cm, that is, $d/L=0.1$ and Sc=7. Superimposed as a dashed line is the distribution given in Eq. (37) with the reduced times $t/\langle t_s\rangle$ reported in the inset for each downstream location.

$$P(C,t)=\frac{\tilde{t}}{\nu}\frac{C^{-(1+\nu)/\nu}}{(C^{-1/\nu}-1)^2}\exp\left(-\frac{\tilde{t}}{C^{-1/\nu}-1}\right), \tag{37}$$

where $\tilde{t}\equiv t/\langle t_s\rangle$. The shape for $P(C,t)$ in Eq. (37) is fitted to the measured distribution with $t/\langle t_s\rangle$ as only fitting parameter (since $\nu=5/2$). The result of the fit is shown in Fig. 10, and the value of the fitting parameter is reported in the inset.

The change in variables $c=C^{-1/\nu}-1$ allows one to compute all the moments $\langle C^q\rangle$ of $P(C)$ as

$$\langle C^q\rangle=\int_0^1 C^qP(C)dC=\tilde{t}\int_0^\infty\frac{(1+c)^{\nu q}}{c^2}e^{-\tilde{t}/c}dc, \tag{38}$$

which are given by

$$\langle C^q\rangle=\Gamma(1+\nu q)U(\nu q,0,\tilde{t}), \tag{39}$$

where Γ and U are the gamma and the confluent hypergeometric functions, respectively. The asymptotic behavior in time is $\langle C^q\rangle\overset{t\to\infty}{\to}\Gamma(1+\nu q)t^{-\nu q}$,[60] so that the width of the distribution becomes on the order of the mean,

$$\frac{\langle C^2\rangle}{\langle C\rangle^2}\sim\frac{\Gamma(1+2\nu)}{\Gamma(1+\nu)^2}\overset{\nu=5/2}{\to}\frac{512}{15\pi}\approx 10.8, \tag{40}$$

consistent with the value measured in Fig. 4. As can be seen in Fig. 10, Eq. (37) fits the experimental distributions over the entire concentration range. The slight mismatch at large excursion reflects the fact that sheets do slightly interact in this flow and aggregate in a way discussed in Ref. 9, but in an extent that does not alter much $P(C,t)$.

Of particular interest is the behavior of the distribution of Eq. (37) around its inflection point as this makes contact with the measurements presented in Sec. II. The local slope at that point was found to steepen linearly in time, with a prefactor depending on the scalar diffusivity (Fig. 5). The shape of $P(C)$ about its inflection point (in log-lin scales) is essentially dominated by the exponential factor $\exp[-\tilde{t}/(C^{-1/\nu}-1)]$ so that $\partial^2\ln P(C)/\partial C^2=0$ for

$$C^* = \left(\frac{\nu-1}{\nu+1}\right)^{\nu} \tag{41}$$

and that

$$\left.\frac{\partial \ln P}{\partial C}\right|_{C^*} = -\frac{(\nu-1)^2}{4\nu}\left(\frac{\nu+1}{\nu-1}\right)^{\nu+1}\tilde{t}, \tag{42}$$

which actually represents precisely the observed trends for $P(C)$, an exponential shape with an argument increasing in proportion to time like $t/\langle t_s\rangle$, as seen in Fig. 5.

The agreement of the prediction for $P(C,t)$ in Eq. (37) with the experimental measurements indicates *a posteriori* the relevant limits and mechanisms involved in the process.

(a) Individual trajectories result from a complex, time dependent, possibly sequential stirring process; however, the effective stretching rate is dominated by the last step sampled in the distribution, consistent with an effective one-step lengthening process [scenario (1)]: the standard deviation of $P(\ell,t)$ is proportional to its mean.
(b) Consequently, the distribution of mixing times has a single characteristic time scale $\langle t_s\rangle$. It is exponential, as for a Poisson process.
(c) The average growth of material lines is linear, which implies an algebraic decay of the individual concentration levels $C(t)$ with $\nu=5/2$.

As a matter of illustration and comparison with item 4 in Sec. III, let us examine the classical case of log normal stretching, the paradigm of multiplicative processes. We choose to write it for simplicity as

$$\mathcal{P}(\ln \ell,t) = \frac{1}{\sqrt{2\pi t}}\exp\left[-\frac{(\ln \ell - t)^2}{2t}\right] \tag{43}$$

and also choose to link the concentration of a particle to its elongation by

$$C(\ell) = (1+\ell)^{-\nu} \tag{44}$$

with, e.g., $\nu=1$, this particular choice being of no consequence in the sequel. The conservation of probability writes in that case

$$P(C,t)dC = \ell\mathcal{P}(\ln \ell,t)d\ell \tag{45}$$

the multiplicative factor ℓ accounting for the fact that concentration levels contribute to the overall distribution in proportion to the length of their support. Thus,

$$P(C,t) = \frac{1}{C^2\sqrt{2\pi t}}\exp\left\{-\frac{[\ln(1/C-1)-t]^2}{2t}\right\}. \tag{46}$$

The corresponding distributions are shown in Fig. 11 and should be compared to Figs. 3 and 10. Most of the concentration levels pileup around $C=0$, leaving a tail for $P(C,t)$, which decays parallel to itself for successive times t. Clearly and in addition to the arguments given in Sec. III, this model in Eq. (43), which is a paradigm for a sequential sequence of stretching, is inadequate to represent the present observations.

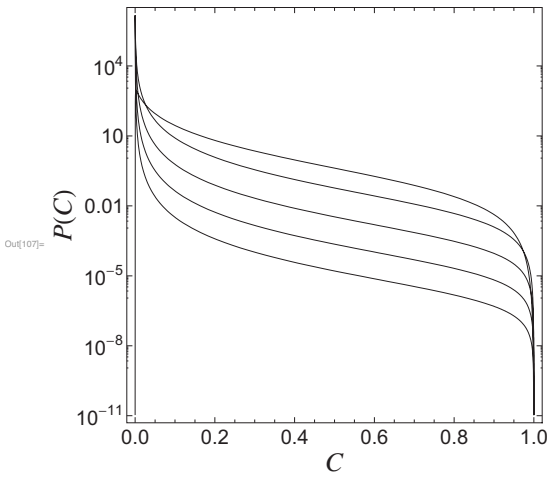

FIG. 11. Concentration distribution $P(C,t)$ of Eq. (46) corresponding to a lognormal distribution of stretching $\mathcal{P}(\ell,t)$ in Eq. (43) for consecutive instants of time (from top to bottom) $t=2,5,10,15,20$. See Figs. 3 and 10 for comparison.

IV. KINETICS

The rate of deformation in time of the distributions $P(C)$ is prescribed by a characteristic time, i.e., the mixing time t_s. For the particular flows we have in the present experiments, where material lines grow linearly in time like σt, in three dimensions, we have shown in Sec. II D that this time writes

$$t_s \sim \frac{1}{\sigma}\left(\frac{\sigma s_0^2}{D}\right)^{1/5}, \tag{47}$$

where s_0 is the initial size of the scalar blobs subsequently stretched into sheets. The composition of the medium solely depends on $x/d=ut/d\sim t/t_s$ in the dispersing mixture suggesting that the mixing time t_s scales like $\sigma^{-1}\sim d/u$ in that case (see also Fig. 7).

The fair *independence* of both the shape of $P(C)$ and of its rate of deformation with the flow Reynolds number (see Fig. 5) suggests that this characteristic time is itself independent of Re, an observation compatible with Ref. 61, finding from direct numerical simulations that the Lagrangian correlation time of the scalar is on the order of the integral time scale, independent of the Reynolds number. That independence is recovered if the size s_0 is itself a function of the elongation rate. The typical scale of the velocity gradient in a turbulent flow is given by the balance between the stretching time σ^{-1} and the time of diffusion of vorticity s_0^2/ν, with ν as the kinematic viscosity of the fluid. This defines

$$s_0 \sim \sqrt{\frac{\nu}{\sigma}} \tag{48}$$

as an analog to the Taylor microscale of the flow.[62,63] This scale represents the transverse size of the sheets initially "peeled-off" from the source by the (unsteady) relative motions in the flow. This observation is consistent with the one-step lengthening process of scenario (1) in Sec. V (see also Refs. 5 and 59 for an example with a sustained shear). With this estimate, the mixing time above becomes

$$t_s \sim \frac{1}{\sigma}\mathrm{Sc}^{1/5}, \tag{49}$$

where $\mathrm{Sc}=\nu/D$ is the Schmidt number and is indeed independent of the Reynolds number. The quantitative comparison in Fig. 10 indicates that $t_s \approx 2d/u$ for $\mathrm{Sc}=7$ in the dispersing mixture with rms velocity such that $u'/u \approx 0.25$, so that $t_s \approx 1.35(d/u)\mathrm{Sc}^{1/5}$ or $t_s \approx 0.4(d/u') \approx \mathrm{Sc}^{1/5}$. A fluid particle emanating from a source of size d such that, say, $d/L \approx 0.1$, has thus experienced roughly $(L/u)/t_s \approx 5$ mixing times during its transit within a local integral scale L. The mixture thus decays appreciably within an essentially stationary stirring field.

A. Cascade bypass

A reformulation of Eq. (49) in the classical framework of sequential processes further illustrates the nature of the "cascade bypass" of the one-step lengthening process scenario depicted here. Let us estimate the velocity difference u_r between two points separated by r as $u_r \sim (\epsilon r)^{1/3}$, and associated persistence time as $t_r \sim r/u_r \sim \epsilon^{-1/3} r^{2/3}$ with $\epsilon = u^3/L$ as the rate of dissipation.[64] Let us label the scales from the injection diameter d as $r_i = dm^{-i}$, where $m > 1$. Then, the time it takes to cascade from d to a (possibly Sc dependent, see Ref. 29) dissipative scale much smaller than d is, according to the standard estimate,[65–67] equal to the sum of the elementary time steps $t_i \sim \epsilon^{-1/3} r_i^{2/3}$ as

$$t_d \sim \sum_{i=0}^{n \gg 1} t_i \sim \epsilon^{-1/3} d^{2/3} \tag{50}$$

and is proportional to $d^{2/3}$, a scaling inconsistent with the present observations (see Fig. 7). The cascade time t_d above thus cannot coincide with the mixing time in the present flow.

If, guided by our discussion in Sec. III, we assume that a blob is distorted not only by the motions matching its own spatial scale, but by *all the scales which are larger than its own size,* one may anticipate that the time it takes for a blob of initial size d to be dissipated reads as

$$t_s \sim \frac{d}{\Sigma_{r_i > d} u_i} f(\mathrm{Sc}), \tag{51}$$

where $f(\mathrm{Sc})$ is a suitable function of the Schmidt number depending on the nature of the large scale distortion motion (see Sec. II D). In this vision, motions at scale $r_i < d$ do contribute to corrugate and chop-off the initial blob, but doing so they generate small stripes that immediately reconnect with neighboring stripes, thus forming "bundles" of stripes carrying essentially the initial blob scalar variance, therefore not contributing much to dissipation.[9,68] Motions at scales $r_i > d$ do, however, distort the blob as a whole and contribute efficiently to its dissipation in the diluting medium, as seen in Fig. 12. Labeling now the scales from the integral scale L as $r_i = Lm^{-i}$, one has $d = Lm^{-i_d}$ and $\Sigma_{r_i > d} u_i = u \Sigma_0^{i_d} m^{-i/3} \sim u$ and thus

$$t_s \sim \frac{d}{u} f(\mathrm{Sc}), \tag{52}$$

consistent with Fig. 7. The function $f(\mathrm{Sc})$ is discussed below.

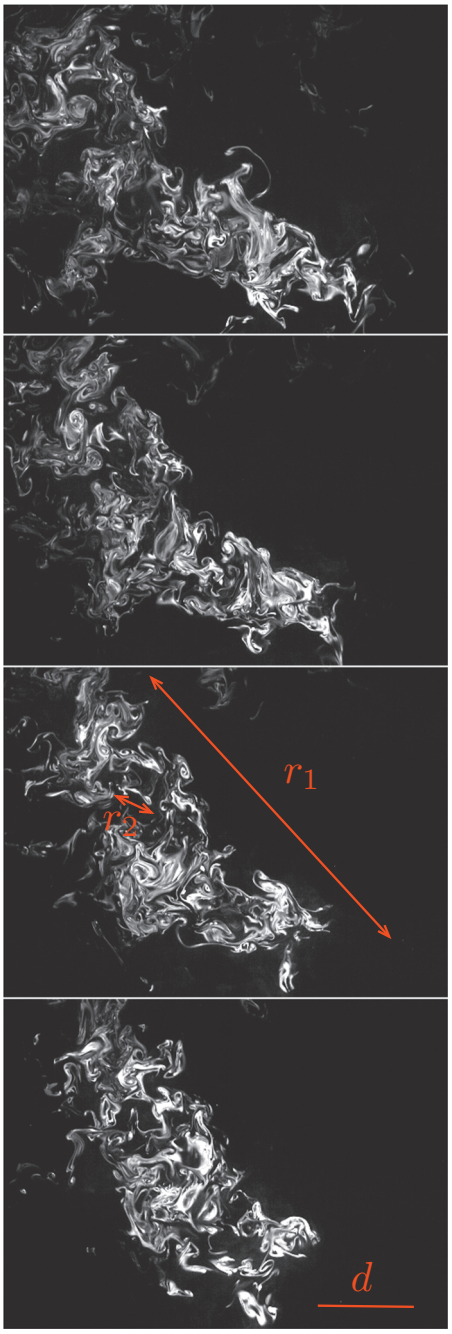

FIG. 12. (Color) Cascade bypass: series of snapshots showing the deformation of a blob in the flow (Sc=2000). The time interval between the images is 0.05 s, and the scale bar of the injection diameter $d=8$ mm is shown on the first image at the bottom. The length scales r_1 and r_2 are such that $r_2 < d < r_1$. The small scale activity of the flow ($r<d$) does not contribute much to the scalar variance decay while larger scales ($r>d$) distort the blob as a whole.

B. Power law versus exponential

Although the flow is turbulent, material lines grow in proportion to time instead of exponentially. This apparent power law has several causes and may be interpreted as a transient effect reflecting the birth of an ultimate, genuine exponential regime: $e^{\sigma t} \approx 1+\sigma t$ at short times. The essentially identical descriptions between the exponential and the power law stretching is further assessed by the Schmidt number dependence $f(\mathrm{Sc})$ of the mixing time revealed, for instance, by the slopes $\alpha \sim f(\mathrm{Sc})^{-1}$ of the histograms $P(C)$ in Fig. 5. The exponential stretching anticipates $\alpha \sim \ln(\mathrm{Sc})^{-1}$, while the linear stretching in three dimensions rather predicts $\alpha \sim \mathrm{Sc}^{-1/5}$, as shown in Sec. II D. As can be seen from Fig. 6, deciding between the two trends is a matter of mood, although the Schmidt number varies on three orders of magnitude. The indecidability comes from the fact that a weak power law (in the present case 1/5) mimics a logarithmic behavior. In other words, looking solely at the Sc dependence of t_s cannot discriminate what kind of underlying flow produces mixing.

The difference is, however, made clear from the measurement of the material lines growth (Sec. II C), and from the direct study of particle dispersion in the flow, demonstrating with no ambiguity that the flow is of a lengthening type (scenario 1) and not of an exponential type.

V. CONCLUSION

The evolution of the concentration level C of a fluid particle in a deforming substrate results from the balance between the substrate rate of deformation and molecular diffusion. The microscopic associated problem is solved in closed form (Sec. II D), illustrating the central concept of the *mixing time* t_s.

The natural randomness among the fluid particles net elongation at a given instant of time induces a distribution of the mixing times from which molecular diffusion becomes effective in erasing the concentration differences. This ingredient, analyzed in Sec. III, has been found to represent very accurately the evolution of the concentration distribution of $P(C,t)$ in an ever dispersing mixture. Its shape and rate of deformation are found to depend on a single, Schmidt number dependent average time scale $\langle t_s \rangle$ (Sec. II).

The analysis suggests that the mixture composition results from a one-step lengthening process distributed among the sheets, as opposed to a sequential cascade of uncorrelated stretching. It infers a prediction for the corresponding distribution of the mixing times [Eq. (33)], consistent with earlier predictions,[13–15,59] and finally a detailed analytic description of $P(C,t)$ [Eq. (37)].

The ever dispersing limit reveals, through the simple measurement of $P(C,t)$, the distribution of individual trajectories inherent to turbulent motions within the mixture among fluid particles when they evolve essentially independent of each other in the medium. This is no longer true when the spatial density of the particles is increased so that their mutual interaction is enforced. The composition $P(C,t)$ given in Eq. (37) is only valid for a single plume dispersing in a large scale stirring field. As soon as multiple sources are present, the picture is different. More generally, a set of constantly overlapping and merging sheets selects a different route toward uniformity, which has been examined in Ref. 9.

ACKNOWLEDGMENTS

We are indebted to Jean-Paul Barbier Neyret for his decisive help with data acquisition. Over the past ten years or so, this work has been supported by the Société Européenne de Propulsion (SEP) under Contract No. 910023, the Centre National d'Études Spatiales (CNES) under Contract No. 02-0485-00, Centre National de la Recherche Scientifique (CNRS), and Agence Nationale de la Recherche (ANR) through Grant No. ANR-05-BLAN-0222-01.

[1] B. Castaing, G. Gunaratne, F. Heslot, L. Kadanoff, A. Libchaber, S. Thomae, X.-Z. Wu, S. Zaleski, and G. Zanetti, "Scaling of hard thermal turbulence in Rayleigh–Benard convection," J. Fluid Mech. **204**, 1 (1989).
[2] Jayesh and Z. Warhaft, "Probability distributions of a passive scalar in grid-generated turbulence," Phys. Rev. Lett. **67**, 3503 (1991).
[3] Jayesh and Z. Warhaft, "Probability distributions, conditional dissipation, and transport of passive temperature fluctuations in grid-generated turbulence," Phys. Fluids A **4**, 2292 (1992).
[4] S. T. Thoroddsen and C. W. Van Atta, "Exponential tails and skewness of density-gradient probability density functions in stably stratified turbulence," J. Fluid Mech. **244**, 547 (1992).
[5] E. Villermaux and H. Rehab, "Mixing in coaxial jets," J. Fluid Mech. **425**, 161 (2000).
[6] M. Holzer and E. D. Siggia, "Turbulent mixing of a passive scalar," Phys. Fluids **6**, 1820 (1994).
[7] B. S. Williams, D. Marteau, and J. P. Gollub, "Mixing of a passive scalar in magnetically forced two-dimensional turbulence," Phys. Fluids **9**, 2061 (1997).
[8] M. C. Jullien, P. Castiglione, and P. Tabeling, "Experimental observation of Batchelor dispersion of passive tracers," Phys. Rev. Lett. **85**, 3636 (2000).
[9] J. Duplat and E. Villermaux, "Mixing by random stirring in confined mixtures," J. Fluid Mech. **617**, 51 (2008).
[10] A. Groisman and V. Steinberg, "Efficient mixing at low Reynolds numbers using polymer additives," Nature (London) **410**, 905 (2001).
[11] C. Simonnet and A. Groisman, "Chaotic mixing in a steady flow in a microchannel," Phys. Rev. Lett. **94**, 134501 (2005).
[12] E. Villermaux, A. D. Stroock, and H. A. Stone, "Bridging kinematics and concentration content in a chaotic micromixer," Phys. Rev. E **77**, 015301(R) (2008).
[13] B. I. Shraiman and E. D. Siggia, "Lagrangian path integrals and fluctuations in random flows," Phys. Rev. E **49**, 2912 (1994).
[14] M. Chertkov, G. Falkovich, I. Kolokolov, and V. Lebedev, "Statistics of a passive scalar advected by a large scale two-dimensional velocity field: Analytic solution," Phys. Rev. E **51**, 5609 (1995).
[15] E. Balkovsky and A. Fouxon, "Universal long-time properties of Lagrangian statistics in the Batchelor regime and their application to the passive scalar problem," Phys. Rev. E **60**, 4164 (1999).
[16] D. T. Son, "Turbulence decay of a passive scalar in the Batchelor limit: Exact results from a quantum-mechanical approach," Phys. Rev. E **59**, R3811 (1999).
[17] J. Kalda, "Simple model of intermittent passive scalar turbulence," Phys. Rev. Lett. **84**, 471 (2000).
[18] D. R. Fereday and P. H. Haynes, "Scalar decay in two-dimensional chaotic advection and Batchelor-regime turbulence," Phys. Fluids **16**, 4359 (2004).
[19] J. Sukhatme and R. T. Pierrehumbert, "Decay of passive scalars under the action of single scale smooth velocity fields in bounded two-dimensional domains: From non-self-similar probability distribution functions to self-similar eigenmodes," Phys. Rev. E **66**, 056302 (2002).
[20] P. Welander, "Studies on the general development of motion in a two-dimensional, ideal fluid," Tellus **7**, 141 (1955).
[21] C. Eckart, "An analysis of the stirring and mixing processes in incompressible fluids," J. Mar. Res. **7**, 265 (1948).
[22] B. I. Shraiman and E. D. Siggia, "Scalar turbulence," Nature (London) **405**, 639 (2000).

[23]G. Falkovich, K. Gawedzki, and M. Vergassola, "Particles and fields in fluid turbulence," Rev. Mod. Phys. **73**, 913 (2001).
[24]E. Ott and T. M. Antonsen, "Chaotic convection and the fractal nature of passive scalar gradients," Phys. Rev. Lett. **61**, 2839 (1988).
[25]A. Celani, M. Martins Afonso, and A. Mazzino, "Point-source scalar turbulence," J. Fluid Mech. **583**, 189 (2007).
[26]L. Danaila and R. A. Antonia, "Spectrum of a passive scalar in moderate Reynolds number homogeneous isotropic turbulence," Phys. Fluids **21**, 111702 (2009).
[27]T. M. Antonsen, Jr., Z. Fan, E. Ott, and E. Garcia-Lopez, "The role of chaotic orbits in the determination of power spectra of passive scalars," Phys. Fluids **8**, 3094 (1996).
[28]E. Gouillart, N. Kuncio, O. Dauchot, B. Dubrulle, S. Roux, and J.-L. Thiffeault, "Walls inhibit chaotic mixing," Phys. Rev. Lett. **99**, 114501 (2007).
[29]E. Villermaux, C. Innocenti, and J. Duplat, "Short circuits in the Corrsin–Oboukhov cascade," Phys. Fluids **13**, 284 (2001).
[30]A. Celani, M. Cencini, M. Vergassola, E. Villermaux, and D. Vincenzi, "Shear effects on passive scalar spectra," J. Fluid Mech. **523**, 99 (2005).
[31]E. Villermaux and C. Innocenti, "On the geometry of turbulent mixing," J. Fluid Mech. **393**, 123 (1999).
[32]A. Lavertu and L. Mydlarski, "Scalar mixing from a concentrated source in a turbulent channel flow," J. Fluid Mech. **528**, 135 (2005).
[33]G. I. Taylor, "Diffusion by continuous movements," Proc. London Math. Soc. **s2-20**, 196 (1922).
[34]K. R. Sreenivasan, "Fractals and multifractals in fluid turbulence," Annu. Rev. Fluid Mech. **23**, 539 (1991).
[35]H. J. Catrakis and P. E. Dimotakis, "Mixing in turbulent jets: Scalar measures and isosurface geometry," J. Fluid Mech. **317**, 369 (1996).
[36]R. Betchov, "An inequality concerning the production of vorticity in isotropic turbulence," J. Fluid Mech. **1**, 497 (1956).
[37]S. S. Girimaji and S. B. Pope, "Material-element deformation in isotropic turbulence," J. Fluid Mech. **220**, 427 (1990).
[38]J. Duplat and E. Villermaux, "Persistency of material element deformation in isotropic flows and growth rate of lines and surfaces," Eur. Phys. J. B **18**, 353 (2000).
[39]J. M. Ottino, *The Kinematics of Mixing: Stretching, Chaos, and Transport* (Cambridge University Press, Cambridge, 1989).
[40]K. A. Buch, Jr. and W. J. A. Dahm, "Experimental study of the fine-scale structure of conserved scalar mixing in turbulent shear flows. Part 1. $sc \gg 1$," J. Fluid Mech. **317**, 21 (1996).
[41]M. A. Levèque, "Les lois de la transmission de la chaleur par convection," Ann. Mines **13**, 201 (1928).
[42]W. D. Mohr, R. L. Saxton, and C. H. Jepson, "Mixing in laminar-flow systems," Industrial and Engineering Technology **49**, 1855 (1957).
[43]F. E. Marble and J. E. Broadwell, "The coherent flame model for turbulent chemical reaction," Project SQUID, Technical Report No. TRW-9-PU, 1977.
[44]W. E. Ranz, "Application of a stretch model to mixing, diffusion and reaction in laminar and turbulent flows," AIChE J. **25**, 41 (1979).
[45]P. B. Rhines and W. R. Young, "How rapidly is a passive scalar mixed within closed streamlines," J. Fluid Mech. **133**, 133 (1983).
[46]F. E. Marble, in *Chemical Reactivity in Liquids: Fundamental Aspects*, edited by M. Moreau and P. Turq (Plenum, New York, 1988).
[47]C. J. Allègre and D. L. Turcotte, "Implications of a two-component marble-cake mantle," Nature (London) **323**, 123 (1986).
[48]D. Beigie, A. Leonard, and S. Wiggins, "A global study of enhanced stretching and diffusion in chaotic tangles," Phys. Fluids A **3**, 1039 (1991).
[49]P. Meunier and E. Villermaux, "How vortices mix," J. Fluid Mech. **476**, 213 (2003).
[50]A. Fannjiang, S. Nonnenmacher, and L. Wolonski, "Dissipation time and decay of correlations," Nonlinearity **17**, 1481 (2004).
[51]P. E. Dimotakis and H. J. Catrakis, in *Mixing Chaos and Turbulence*, edited by H. Chaté, E. Villermaux, and J. M. Chomaz (Kluwer Academic, New York/Plenum, New York, 1999).
[52]E. S. Szalai and F. J. Muzzio, "Predicting microstructure in three-dimensional chaotic systems," Phys. Fluids **15**, 3274 (2003).
[53]G. A. Voth, G. Haller, and J. P. Gollub, "Experimental measurements of stretching fields in fluids," Phys. Rev. Lett. **88**, 254501 (2002).
[54]S. Kida and S. Goto, "Line statistics: Stretching rate of passive lines in turbulence," Phys. Fluids **14**, 352 (2002).
[55]J.-P. Bouchaud and M. Potters, *Theory of Financial Risks and Derivative Pricing* (Cambridge University Press, Cambridge, 2003).
[56]G. Boffetta and I. M. Sokolov, "Statistics of two-particle dispersion in two-dimensional turbulence," Phys. Fluids **14**, 3224 (2002).
[57]M. K. Rivera and R. E. Ecke, "Pair dispersion and doubling time statistics in two-dimensional turbulence," Phys. Rev. Lett. **95**, 194503 (2005).
[58]S. N. Coppersmith, C. h. Liu, S. Majumdar, O. Narayan, and T. A. Witten, "Model for force fluctuations in bead packs," Phys. Rev. E **53**, 4673 (1996).
[59]E. Villermaux, C. Innocenti, and J. Duplat, "Histogramme des fluctuations scalaire dans le mélange turbulent transitoire," C. R. Acad. Sci., Ser. IIb Mec. Phys. Astron. **326**, 21 (1998).
[60]M. Abramowitz and I. A. Stegun, *Handbook of Mathematical Functions* (Dover, New York, 1964).
[61]P. K. Yeung, "Lagrangian characteristics of turbulence and scalar transport in direct numerical simulations," J. Fluid Mech. **427**, 241 (2001).
[62]G. I. Taylor, "Statistical theory of turbulence. Part I," Proc. R. Soc. London, Ser. A **151**, 421 (1935).
[63]S. B. Pope, *Turbulent Flows* (Cambridge University Press, Cambridge, 2000).
[64]U. Frisch, *Turbulence* (Cambridge University Press, Cambridge, 1995).
[65]S. Corrsin, "On the spectrum of isotropic temperature fluctuations in an isotropic turbulence," J. Appl. Phys. **22**, 469 (1951).
[66]L. Onsager, "Statistical hydrodynamics," Nuovo Cimento **6**, 279 (1949).
[67]S. Corrsin, "The isotropic turbulent mixer: Part II. Arbitrary Schmidt number," AIChE J. **10**, 870 (1964).
[68]E. Villermaux and J. Duplat, "Coarse grained scale of turbulent mixtures," Phys. Rev. Lett. **97**, 144506 (2006).